J Therm Anal Calorim
DOI 10.1007/s10973-016-5391-0

Thermal properties and combustion behaviors of flame-retarded glass fiber-reinforced polyamide 6 with piperazine pyrophosphate and aluminum hypophosphite

Xiong Xiao[1] · Shuang Hu[1] · Jinguo Zhai[1] · Tao Chen[1] · Yongyi Mai[1]

Received: 1 November 2015 / Accepted: 7 March 2016

Abstract Flame-retardant glass fiber-reinforced PA6 (GFPA6) composites were prepared by incorporating the mixture of piperazine pyrophosphate (PAPP) and aluminum hypophosphite (AHP) into GFPA6. From the results of UL-94 test, limiting oxygen index (LOI) and microscale combustion calorimetry (MCC) tests, the as-obtained composites exhibited significantly enhanced flame retardancy including higher LOI values, better UL94 rating (V-0 for 18.0 mass% PAPP/AHP mixture), and decreased peak heat release rate and total heat release. And PA6-4 with a 4/1 mass ratio of PAPP to AHP reached the highest LOI value. The influence of PAPP/AHP on the decomposition pathway of GFPA6 was discussed based on TG and TG-FTIR analysis. The interaction between PAPP/AHP and GFPA6 altered the decomposition pathway of GFPA6 resulting in the formation of compact char layer, high thermal stability within high-temperature region, and weak intensities of a variety of pyrolysis gas products. Meanwhile, the thermomechanical property data revealed the storage modulus of samples were increased with increasing PAPP/AHP content, whereas the glass transition temperatures were reduced gradually. Moreover, the results of scanning electron microscope illustrated that the introduction of PAPP/AHP mixture can promote the formation of compact char layer and change the surface element composition of the char.

✉ Shuang Hu
hushuang8427@gmail.com

[1] Shanghai Research Institute of Chemical Industry, No. 345 East Yunling Road, Shanghai 200062, People's Republic of China

Keywords Combustion behavior · Flame retardant · Mechanism · Glass fiber-reinforced polyamide 6

Introduction

Polyamide 6, as one of the most important engineering plastics, has been widely used in electronic industry and automobile industry. As well known, pure polyamides (especially PA6) are endowed with relatively high tensile strength, good aging resistance, high ductility, good chemical resistance, good abrasion, low friction coefficient, good electrically insulating property and easy processing properties [1–3]. Nevertheless, polyamide 6 also has some shortcomings such as high moisture absorptivity, poor dimensional stability, low heat distortion temperature, poor low-temperature impact strength and easy flammability. Thus, reinforcing modification needs to be used on the virgin polyamide materials. Most industrial applications require the reinforced polyamide composites. Industrially, glass fiber (GF) is the additive which is typically utilized in reinforcing polyamide 6 materials due to its low cost, good compatibility, and simple preparation process. The dimensional stability, heat distortion temperature, impact resistance, resistance to chemical solvent, aging resistance, and moisture absorption resistance of the corresponding composites following the glass fiber are significantly improved [4, 5]. However, flame retarding of GFPA6 is much more difficult to reach than that of PA6 owing to the "candlewick effect," which greatly limits their applications in electric industries, including electrical connectors, switch components, wire ties, and electrical housings. This comes from that the introduction of glass fibers can evidently accelerate the combustion and thus undermine the capability of self-extinguishment of PA6 matrix [6].

Published online: 24 March 2016

Traditionally, halogen-containing flame retardants have taken up a huge market in last decades and are often industrially used in decreasing the combustibility of glass fiber-reinforced PA6 materials. Nonetheless, the halogenated FRs also cause corrosion to the processing equipment and generate corrosive and toxic combustion products (especially the "dioxin") during combustion, which limits their further applications in some fields [7].

Therefore, halogen-free flame-retarding GFPA6 has attracted many attempts. Halogen-free retardants mainly include phosphorus-containing flame retardant (FR), nitrogen-containing FR, and inorganic FR [8–10]. However, it is difficult to achieve a high flame-retarded classification for polyamides with a low loading of these compounds. Metal phosphinates are proven to be effective flame retardants activating in both condensed and gaseous phases. In recent years, aluminum hypophosphite (AHP, Fig. 1) has been employed as efficient flame retardant and widely applied in engineering plastics. Zhao and Li [11] reported that AHP has low flame-retardant efficiency in materials by its alone, which means some synergists are required to exert better performance. Thus, synergistic effects of melamine cyanurate (MCA) and AHP in PBT [12], ABS [13] and PA6 [14] have been studied, which needed over 20 mass% total loading to achieve UL94 V-0 rating. The incorporation of aluminum phosphinate, melamine polyphosphate (MPP), and zinc borate also presented high flame-retarding efficiency in glass fiber-reinforced PA66 [15]. Howbeit, there are also some defects on AHP. As well known, releasing toxic and combustible gas (phosphine, PH_3) during combustion is the main defect of AHP. Though this system can reach a good flame-retarding result, but the high content of AHP in this system increases the releasing of PH_3 and cost (the preparation of organic phosphinate salts on industrial scale is relatively complex and expensive) [16]. Furthermore, no interested attempts about decreasing the content of AHP in those systems for flame-retarding GFPA6 were reported.

In our previous work, piperazine pyrophosphate (PAPP, Fig. 1) was synthesized by copolymerization [17]. PAPP that contains nitrogen and phosphorus shows high initial degradation temperature, high phosphorus element content, and good char-forming property, which makes it suitable to the preparation of flame-retarding GFPA6 composites. Meanwhile, PAPP is possible to be a commercial product due to its simple preparation process, low cost, moisture absorption resistance, and good availability. Theoretically, the phosphoric acid decomposing from PAPP can accelerate the cross-linked reaction in condensed phase; meanwhile, the AHP can form more uniform and compact char layer on the surface of materials and eliminate the dripping phenomenon. Thus, PAPP and AHP may exhibit excellent flame-retarding efficiency in GFPA6 materials.

The purpose of this paper is to study the synergistic effect between PAPP (as the main component) and AHP (as the synergistic ingredient) in the flame-retarding system for GFPA6 materials, for significantly decreasing the release of PH_3 and maintaining the flame-retarding rating. This system is different from the previous system in which AHP is the main ingredient reported by the literatures. We partially replaced the PAPP with AHP to more fully understand the flame-retarding activity of PAPP/AHP in GFPA6 composites. The fire retardation properties and thermal stability behaviors of GFPA6/PAPP/AHP composites were investigated by limiting oxygen index (LOI), UL94 vertical test, thermogravimetric analysis (TG), microscale combustion calorimeter (MCC) test, thermogravimetry/infrared spectrum (TG-FTIR) analysis, dynamic mechanical analysis (DMA), and scanning electron microscopy (SEM). Meanwhile, the synergistic mechanism between PAPP and AHP was also discussed.

Experimental

Materials

Polyamide 6 (PA6, YH800) was supplied by Baling Petrochemical Co., China. AHP was purchased from Hubei Tian'Hu Chemical Co., Ltd., China. Piperazine phosphate,

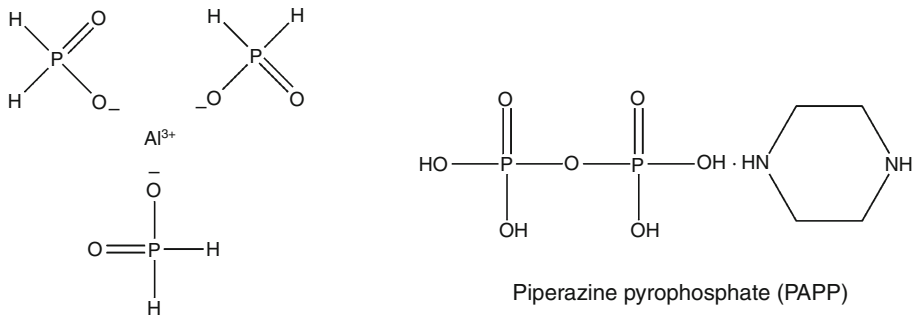

Fig. 1 Chemical structure of AHP and PAPP

phosphate, and xylene (chemically pure) were supplied by Chengdu Kelong Chemical Plant, China.

Synthesis of PAPP

A certain amount of piperazine phosphate and phosphate (mole ratio of 1:1) were added into the heat xylene solution with a molecular structure of C_8H_{10}, followed by a continued reaction in water bath for a given time at a certain temperature (150–300 °C) and rotor speed of 40 rpm after completion of addition of piperazine phosphate and phosphate. After completion of the reaction, the reaction mixture was cooled down to room temperature, filtrated, and then dried. The obtained products were finally pulverized to <100 μm for the subsequent use. We called the reaction product as PAPP (Schme 1).

Table 1 Compositions of flame-retarding materials

Sample	Components			
	PA6/mass%	GF/mass%	PAPP/mass%	AHP/mass%
PA6-0	70	30	0	0
PA6-1	50	30	20	0
PA6-2	50	30	13.33	6.67
PA6-3	50	30	15	5
PA6-4	50	30	16	4
PA6-5	50	30	16.63	3.33
PA6-6	50	30	17.15	2.85
PA6-7	50	30	17.5	2.5
PA6-8	50	30	0	20
PA6-9	52	30	14.4	3.6
PA6-10	54	30	12.8	3.2

Preparation of FR-GFPA6 Composites

The composites were prepared on an internal mixer (SU-70, SU YAN Science and Technology co., Ltd) with the temperature of 230 °C and rotor speed of 40 rpm. After the mixing, the samples were hot pressed in a Plate Vulcanizing Press (XLB-350, Shanghai First Rubber Machinery Works) at 240 °C under 10 Mpa for 5 min into sheets. The compositions of all samples are shown in Table 1.

Characterization

The Fourier transform infrared (FTIR) spectra of samples were collected using a Nicolet 20SXB FTIR spectrometer.

The proton nuclear magnetic resonance spectroscopy (^{1}H NMR) was performed on a Varian Unity Inova 500 NB spectrometer by using $CDCl_3$ as solvent and tetramethylsilane (TMS) as a reference.

The element analysis of the sample was used an Elementar Vario EL III. About 2.0 mg of the sample was taken and the nitrogen, carbon, hydrogen and phosphorus elements were analyzed.

The flammability of the sample was determined on a HC-2 limiting oxygen index instrument with test bars of size $100 \times 6.5 \times 3.2$ mm^3, according to the ASTM standard D2863. The UL94 test was measured on a horizontal and vertical burning tester with sheets dimension of $127 \times 12.7 \times 1.6$ mm^3 using the standard America National UL 94 test ASTM D3801.

Thermogravimetric properties of the samples were performed using a NETZSCH Q209 thermal analyzer with N_2 flow rate of 20 mL min^{-1}. About 10.0 mg of sample was put in an alumina crucible with a heating rate of 20 °C min^{-1} at the temperature range of 50–700 °C. Values for residues were taken at 700 °C.

Combustion properties were performed on a microscale combustion calorimeter (IL60050, MCC-2, Govmark), according to ASTM D 7309-7 standard procedures. The sample was heated from ambient temperature to 800 °C and the heating rates were set as 40 °C min^{-1} (80 % nitrogen atmosphere, 20 % oxygen atmosphere, flow rate of 100 mL min^{-1}).

TG was coupled with a Tensor 27 FTIR spectrometer (Bruker, Germany) for TG-FTIR investigations. A transfer tube with an inner diameter of 1 mm (heated to 230 °C) linked the TG and the infrared cell (heated to 230 °C). The infrared spectrometer was used at an optical resolution of 4 cm^{-1}. Single spectra were chosen to discern the evolved gases. The identification was based on characteristic peaks demonstrating chemical structure.

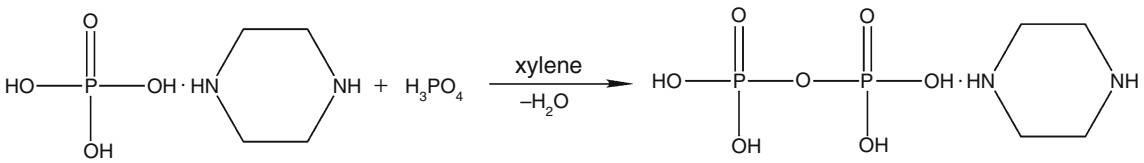

Piperazine phosphate

Piperazine pyrophosphate (PAPP)

Scheme 1 Synthesis route of PAPP

Mechanical properties of the FR materials were obtained by means of a PerkinElmer DMA8000 dynamic mechanical analyzer (DMA). The samples were subjected to a controlled sinusoidal displacement of 0.01 mm at frequencies of 10 Hz in the double-cantilever bending configuration. Besides, the samples were heated from room temperature to 220 °C and the heating rates were set as 5 K min^{-1}. The storage modulus (E'), loss modulus (E'') and damping factor (tan δ) were monitored as a function of temperature.

The surface of residual charred layer was observed by a XL30E scanning electron microscope (SEM). The residual charred layer was from the burned specimen in the UL94 test. The samples to be observed were coated with a conductive gold layer in advance.

Results and discussion

The characterization of PAPP

The chemical structure of PAPP was characterized with FTIR, ^{1}H NMR, and element analysis. Figure 2 presents the FTIR and ^{1}H NMR spectrum of PAPP.

The absorption band of –OH was appearance at 3254 cm^{-1}, as found in Fig. 2a. The peaks at 1211 and 1440 cm^{-1} were assigned to the stretching band of P=O and C–N group, respectively. The peak at 955 cm^{-1} should correspond to the vibration of P–O–P. The bending vibrations at 1637 and 2813 cm^{-1} represented to the N–H in C–N–H group. Meanwhile, the absorption bands for C–H stretching vibration in PAPP appeared at 3000 cm^{-1}. Therefore, it illustrated that PAPP was contained within the synthesized nitrogen–phosphorus flame retardant by the presence of functional groups of PAPP.

Proton nuclear magnetic resonance spectroscopy (^{1}H NMR) measurement was conducted to characterize the obtained PAPP. In Fig. 2b, it can be seen the peak between 4.51 and 4.68 ppm was assigned to the protons of $–CH_2$. Further, the characteristic peak from 3.39 to 3.49 ppm was also been observed, which was attributed to the H protons of D_2O molecule.

Table 2 presents the calculated and experimental contents of elements in products. From Table 2, the theoretical contents of nitrogen, carbon, hydrogen, and phosphorus element were 18.18, 5.30, 10.61 and 23.48 mass%, respectively, while the found percentage contents of nitrogen, carbon, hydrogen and phosphorus element were 17.79, 4.66, 10.55 and 23.28 mass%, respectively, indirectly confirming the almost completely reaction of synthesis. It also can be a strong evidence to characterize the chemical structure of

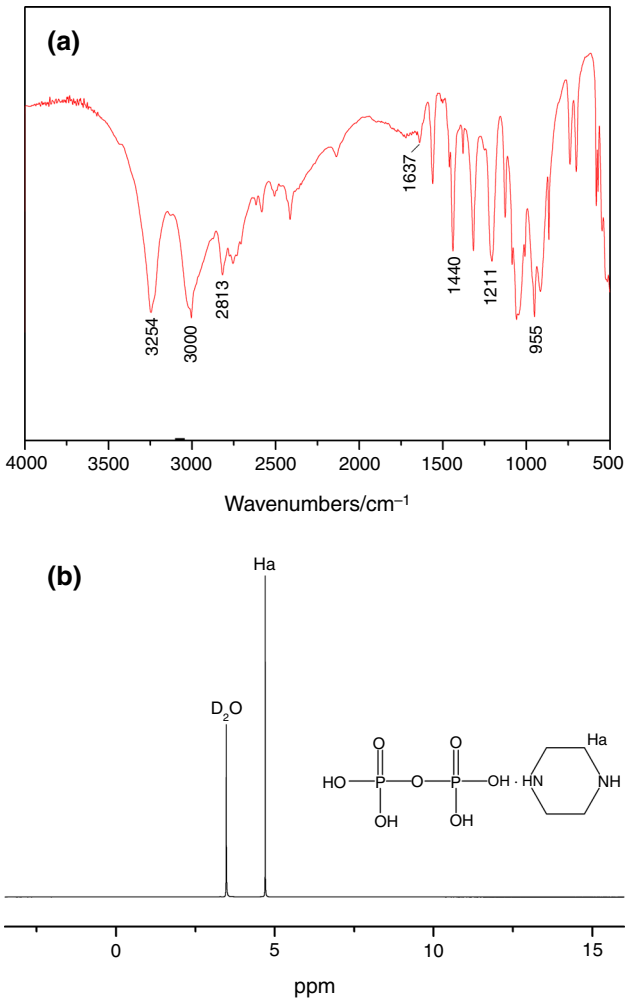

Fig. 2 FTIR (**a**) and ^{1}H NMR (**b**) spectrum of PAPP

Table 2 Element analysis of PAPP

Samples	*C*/mass%	*H*/mass%	*N*/mass%	*P*/mass%
Calculated content	18.18	5.30	10.61	23.48
Experimental content	17.79	4.66	10.55	23.28

PAPP. Unfortunately, all the experimental element content presenting a decrease may be ascribed to the impurities in the samples. Above results indicated that the target product has been synthesized successfully.

Flammability of composites

LOI and UL94 test are essential indicators to evaluate the flammability properties of materials. Table 3 and Fig. 3 show the LOI and UL-94 test results of GFPA6 and its composites with different formulations.

Table 3 Flammability properties of composites

Samples	Parameters		
	LOI/vol%	UL94/1.6 mm	Dripping
PA6-0	23.0	No rating	Yes
PA6-1	28.0	V-2	Yes
PA6-2	30.0	V-1	No
PA6-3	31.5	V-0	No
PA6-4	34.0	V-0	No
PA6-5	33.0	V-0	No
PA6-6	31.0	V-1	No
PA6-7	30.0	V-1	No
PA6-8	27.0	V-1	No
PA6-9	32.0	V-0	No
PA6-10	30.0	V-1	No

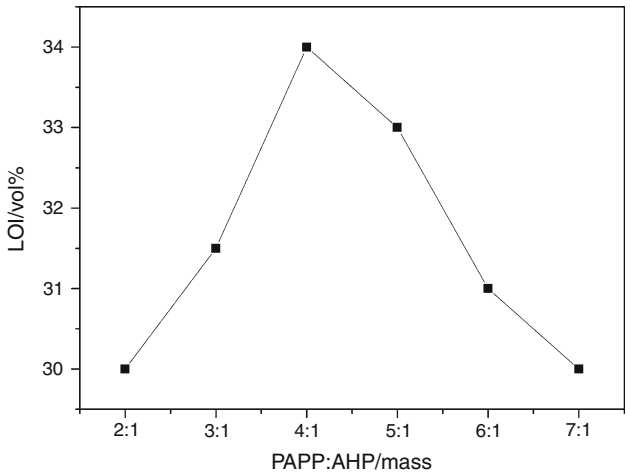

Fig. 3 LOI of different mass ratio of PAPP to AHP in composites

The pure GFPA6 materials are easily flammable along with continual dripping during combustion, and its LOI value is only 23.0 vol%. The LOI values of PAPP/GFPA6 and AHP/GFPA6 with 20 mass% loadings were 28.0 and 27.0 vol%, respectively, and neither can achieve UL-94 V-0 rating. The LOI values and UL-94 rating of FR-GFPA6 composites were remarkably increased when PAPP combined with AHP. The LOI value firstly ascended from 23.0 to 34.0 vol% and then descended from 34.0 to 30.0 vol% with the continuous changes of mass ratio (PAPP:AHP) from 2:1 to 7:1. This may be attributed to the formation of bridges between PAPP and AHP, bringing about a stabilization of the char, which could increase the viscosity of the melt during pyrolysis and combustion. The flame-retardant GFPA6 blend with higher viscosity in the melt state will constrain the volatilization of degradation products and the generation of dripping during the combustion process, contributing to improve the flame retardancy of the obtained composites [18]. Meanwhile, when the mass ratios were 3:1, 4:1 and 5:1, the corresponding specimens with the thickness of 1.6 mm successfully passed UL-94 V-0 flammability rating. Furthermore, the combination of PAPP and AHP reached the highest LOI value of 34.0 vol%, dramatically obtained UL-94 V-0 classification and totally eliminated the dripping phenomenon during combustion based on the mass ratio of 4:1 (PA6-4). Consequently, we took the mass ratio (PAPP:AHP) of 4:1 as the optimal proportion.

The total FR loadings of 18.0 mass% (PA6-9) and 16.0 mass% (PA6-10) that with the optimal proportion (4:1) of PAPP/AHP were added into materials to investigate the minimum FR addition. Experimentally results indicated that V-0 rating was obtained containing 18.0 mass% FR, whereas V-1 rating was only detected with 16.0 mass% FR powder, illustrating 18.0 mass% PAPP/AHP mixtures was the minimum addition to acquire expected results. These results demonstrated that the combination with AHP could remarkably improve the flame-retarding performance of PAPP in GFPA6, and AHP showed a synergistic flame-retardant effect with PAPP.

Thermal stability of composites

TG is one of the most widely used techniques for rapid evaluation of the thermal stability for various polymers [19]. The TG and DTG curves of virgin GFPA6 (sample PA6-0), GFPA6/16.0 mass% FR (sample PA6-10), GFPA6/18.0 mass% FR (sample PA6-9), and GFPA6/20.0 mass% FR (sample PA6-4) system are presented in Figs. 4 and 5; meanwhile the relevant thermal decomposition data are summarized in Table 4.

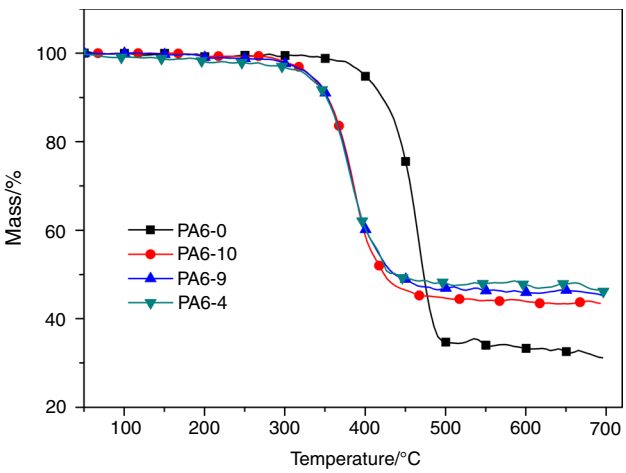

Fig. 4 TG curves of virgin GFPA6 and FR-GFPA6 composites

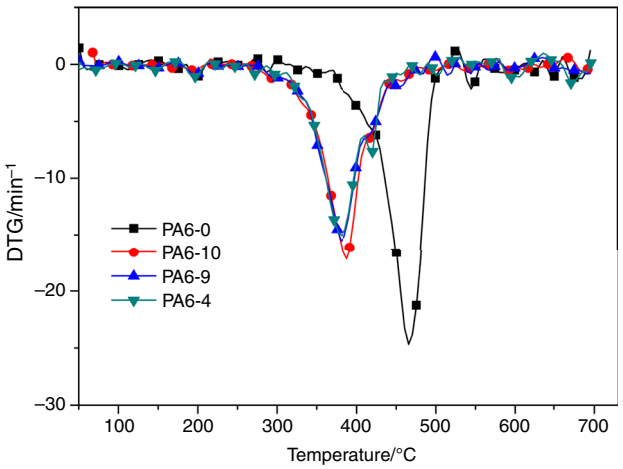

Fig. 5 DTG curves of virgin GFPA6 and FR-GFPA6 composites

The pure GFPA6 began to decompose at 397 °C, the char yield was 31.3 mass% at 700 °C, and the thermal degradation process was only one step attributing to the depolycondensation and cross-linking reaction, as revealed in Fig. 4 and Table 4. The temperature of maxim thermal degradation rate (T_{max}) appeared at 465 °C accompanying with a maximum mass loss rate (MMLR) of 24.8 % min^{-1}. However, the presence of flame retardants reduced the onset temperatures ($T_{5\ \%}$, temperatures at 5 % mass loss) of samples, from 397 to 331 °C, 327 °C, and 312 °C, which was due to the degradation as well as the dehydration of flame retardants. In contrast, when the temperature increased to 500 °C, all FR containing samples exhibited better thermal stability than that of pure GFPA6. Within high-temperature region, PA6-10, PA6-9, and PA6-4 materials obtained increased char residue from 31.3 to 43.4 mass%, 45.1 and 46.2 mass%, respectively, showing better thermal oxidative stability. In addition, the T_{max} of the FR-GFPA6 composites were lower than that of PA6-0 before 465 °C. This decrease may be ascribed to the PAPP/AHP that stimulated the decomposition of PA6 to a considerable degree as well as accelerated the cross-linking reaction [20–22]. Otherwise, the addition of flame retardants remarkably decreased the MMLR to a considerable intensity. With increasing FR contents from 16 to 20 mass%, the MMLR of the corresponding materials decreased according to the following order, i.e. PA6-0 (24.8 % min^{-1}) > material with 16 mass% FRs (17.0 % min^{-1}) > material with 18 mass% FRs (15.6 % min^{-1}) > material with 20 mass% FRs (15.1 % min^{-1}).

As a result, the FR-GFPA6 composites with higher flame-retardant content yielded more protective char layer, which presented higher stability at high temperature. It was well known that char layer can block the transfer of oxygen and heat, thus inhibit thermal decomposition of underlying materials. Therefore, the introduction of PAPP/AHP effectively improved the thermal stability of FR-GFPA6 composites.

MCC test of PA6/FR blends

The method of good choice for performing a real fire is the MCC, developed to predict the flammability behavior of materials in real fire scenarios, due to its good correlation with real fire disasters [23]. Various parameters obtained or carried from experimental MCC results like heat release rate (HRR), total heat release (THR) and peak HRR (PHRR) could be employed to evaluate the developing, spreading, and intensity of fires. The HRR versus temperature curves for FR-GFPA6 are shown in Fig. 6 and the corresponding data is summarized in Table 5.

As shown in Table 5 and Fig. 6, the HRR curve of PA6-0 was characterized by a shoulder from the ignition temperature of 250 °C up until 468 °C where a sharp peak was observed. Compared with PA6-0, the presence of PAPP/AHP significantly decreased the PHRR and THR values. The PHRR of PA6-0 was 377 w g^{-1}, while the PHRR of PA6-10, PA6-9, and PA6-4 were reduced to 280, 270, and 217 w g^{-1}, respectively. In this case, the decrease was identified as the collapse of PAPP/AHP and the development of the intumescent char, which could protect samples. Similarly, the notable reductions in THR values from 18.5 to 14 kJ g^{-1}, 12.8 and 11.0 kJ g^{-1} were also detected. The results implied that the PAPP/AHP can effectively inhibit fire risk of glass-reinforced PA6 composites [24]. This change may be caused by the catalytic action of phosphorus compounds that enabled flame retardant to dehydrate at the lower temperatures, accelerated the formation of char and reduced the release of combustible gas.

Table 4 TG data of virgin GFPA6 and FR-GFPA6 composites

Samples	$T_{5\%}$/°C	T_{max}/°C	MMLR/% min^{-1}	Char residues at 700 °C/mass%
PA6-0	397	465	24.8	31.3
PA6-4	312	369	15.1	46.2
PA6-9	327	382	15.6	45.1
PA6-10	331	384	17.0	43.4

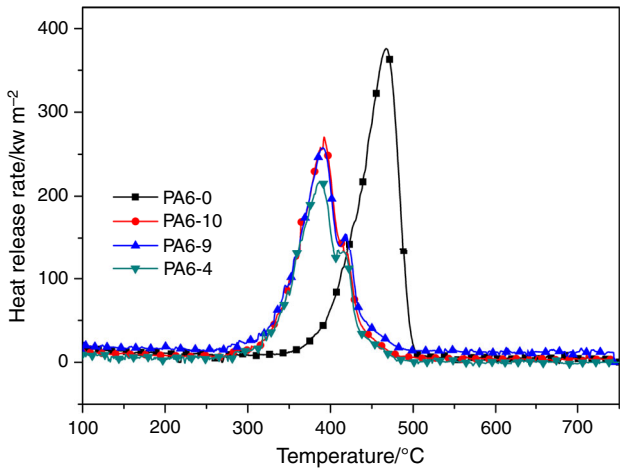

Fig. 6 HRR curves of GFPA6 and FR-GFPA6 samples

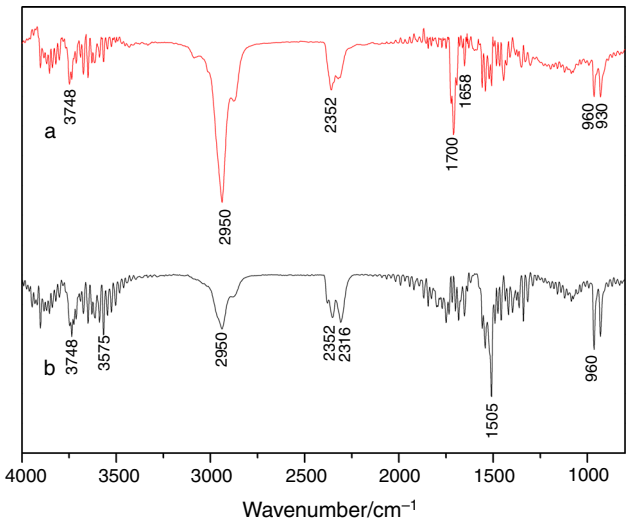

Fig. 7 Evolved gas spectra of TG-FTIR for *a* PA6-0 at 1233 s and *b* PA6-4 at 1060 s

Table 5 MCC data of GFPA6 and FR-GFPA6 composites

Samples	PHRR/w g^{-1}	THR/KJ g^{-1}	T_c/°C
PA6-0	377	18.5	468
PA6-4	217	11	386
PA6-9	270	12.8	389
PA6-10	280	14	391

Consistently, the temperatures at PHRR (T_c) of FR-GFPA6 composites were shifted forward to lower temperature compared with that of PA6-0. Results of Table 5 showed the T_c of PA6-10, PA6-9, and PA6-4 decreased from 468 °C to 391 °C, 389 °C, and 386 °C, correspondingly. This phenomenon was due to the low initial thermal stability of PAPP/AHP mixture.

Evolved gas analysis

In order to obtain information about the evolution of the gas evolved from TG furnace, the TG-FTIR spectra of pyrolysis products for materials (465 °C for PA6-0 corresponded to the spectrum at 1233 s, while 369 °C for PA6-4 corresponded to the spectrum at 1060 s) during the thermal degradation are shown in Fig. 7. The FTIR spectrum of the evolved gases at peak decomposition temperature (Fig. 7a) showed the production of water (3800–3200 cm^{-1} and 1800–1200 cm^{-1}), carbon dioxide (2355–2310 cm^{-1}), and olefinic compounds (930, 960 and 3000–2900 cm^{-1}). The absorbance at 2950 and 1658 cm^{-1} corresponded to hydrocarbons and ε-caprolactam monomer, while the absorbances at 960 and 930 cm^{-1} represented to the evolution of NH_3. It has been found that the model processes involved for PA6 degradation were an intramolecular backbiting process and hydrogen transfer reaction leading to scission of the C–N bond to the amide group. The results fitted well to the literatures [25–27].

According to the results of volatiles produced at peak decomposition, there was a difference between GFPA6 and FR-GFPA6 composites (Fig. 7b). In contrast, the evolved gas analysis of PA6-4 exhibited that the signal intensity was clearly decreased compared with that of PA6-0. Furthermore, the peak of carboxylic acid was not clearly observed. Trace of P–H presence was evidenced by the peak at 2316 cm^{-1} assigning to represent the model degradation product of aluminum hypophosphite. The signal of carbon dioxide became wide, which can significantly dilute the combustible gases generated by matrix in the gaseous phase. The main pyrolysis products of PA6-4 were water (3748 cm^{-1}), hydrocarbons (2950 cm^{-1}), carbon dioxide (2352 cm^{-1}), phosphine (2316 cm^{-1}), and aromatic compounds (1505 cm^{-1}), respectively. A higher overall absorbance at 1505 cm^{-1} was discerned in the case of FR-GFPA6 because of the formation of a large quantity of protective char layer.

The relationship between intensity of characteristic peak and time for volatilized CO_2 and ε-caprolactam are plotted in Fig. 8. Compared with PA6-0, the peak value of carbon dioxide for PA6-4 was reduced 71 %; meanwhile, the release peak width was narrowed (Fig. 8a). This decrease may be attributed to the carbon reaction staying in condensed phase as well as consuming the carbon of the PA6 molecular chain, which resulted in the decrease of carbon dioxide in the gaseous phase. Meanwhile, the biggest shift occurred on the ε-caprolactam release curves (Fig. 8b). The hypophosphorous acid decomposing from AHP led to the formation of a radical; then reacted with ε-caprolactam generated from the heterolytic cleavage of PA6; and finally

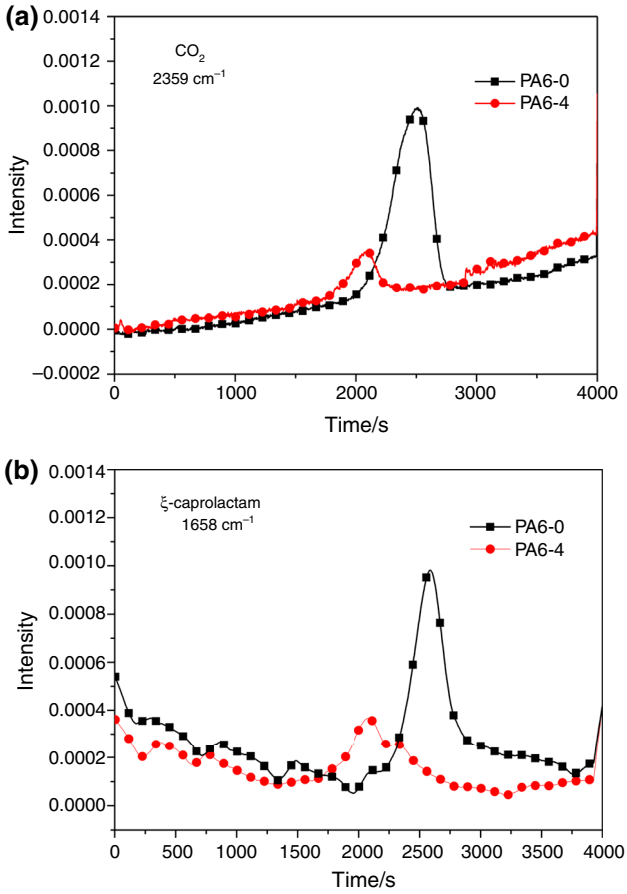

Fig. 8 Decomposition products release rates of PA6-0 and PA6-4 determined by TG-FTIR for **a** carbon dioxide and **b** ε-caprolactam

produced cross-linking materials. The cross-linking products along with $Al_4(P_2O_7)_3$ and $AlPO_4$ directly formed from AHP composed the char-like residue during burning, which could act as a physical barrier to prevent the mass/heat transfer and protect the inner materials away from fire [27]. The evolution of ε-caprolactam was almost affected by PAPP/AHP, meaning a totally pyrolysis process of PAPP/AHP formed compact char residue.

The intensity of phosphine for PA6-8 and PA6-4 was also presented in Fig. 9, for studying the release of toxic gas in gaseous phase. Compared with the narrow and sharp release peak of phosphine for PA6-8, the peak of PA6-4 was wide and short. The release of phosphine decreased by 75 %, convincingly confirming that the interaction of AHP and PAPP can reduce the fire risk. It was in good agreement with what we wanted.

Dynamic mechanical analysis

DMA was used to study the curing behavior of thermosetting resins or composites [28–30]. The storage modulus (E') and loss tangent (tan δ) values of the GFPA6

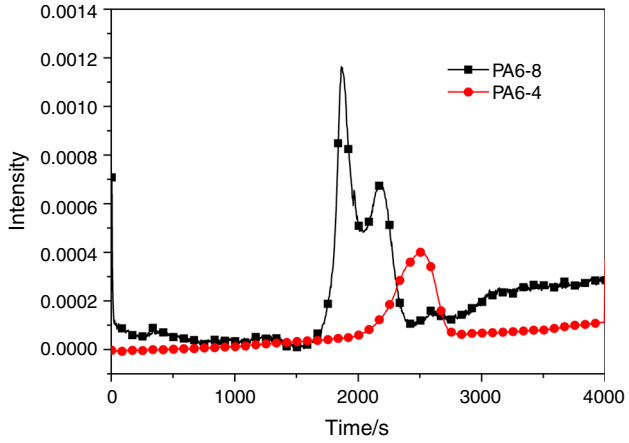

Fig. 9 Intensity of phosphine of PA6-8 and PA6-4

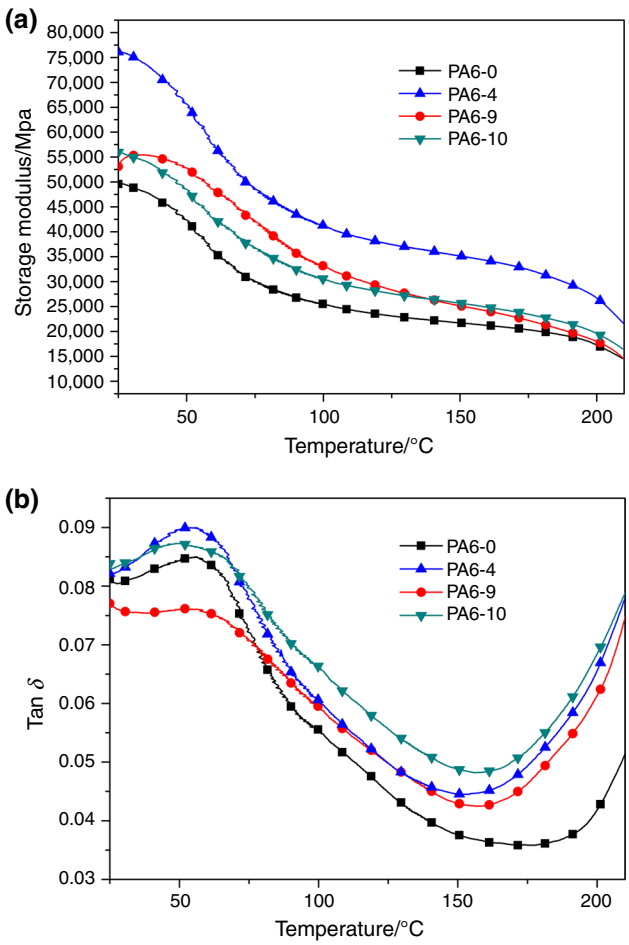

Fig. 10 Dynamic mechanical analysis for **a** storage modulus and **b** loss factor

composites with different FR contents as a function of temperature (30–220 °C) are presented in Fig. 10. Over a wide temperature region, the storage modulus of FR-GFPA6 composites were larger than that of pure GFPA6

matrix, a careful inspection of data evidenced that nearly 12 % values increase taken place. Moreover, it should be noticed that E' ascended with increasing FR contents within the glassy region. This improvement maybe ascribed to the reinforcement effect of AHP (inorganic FR).

The curves of loss factor (tan δ) were also showed in Fig. 10. The glass transition temperatures (T_g) of composites were calculated from the maxima (peak) of tan δ curves [31, 32]. The peak for tan δ within the temperature range of 50–70 °C has been attributed to the T_g of FR-GFPA6 composites. All the FR-GFPA6 composites had T_g above room/ambient temperature making them rigid. Pure GFPA6 matrix had the highest T_g at 58 °C, whereas 16.0 mass% FR/GFPA6 (PA6-10), 18.0 mass% FR/GFPA6 (PA6-9) and 20.0 mass% FR/GFPA6 (PA6-4) decreased to 55, 54 and 50 °C, respectively. One probable reason for this phenomenon can be attributed to the changes of crystallization behavior of FR-GFPA6 blends in the presence of AHP and PAPP. No significant difference on the width of relaxation peaks among all the samples, which confirmed good miscibility between FR and PA6 matrix.

SEM analysis

In generally, the morphology and chemical composition of residue are governed by the flame retardancy mechanism, which has great impact on the actual flame retardancy. The morphologies of the residual char of PA6-0 (without FR) and PA6-4 (with 20 mass% FR) were observed by SEM instrument, as shown in Fig. 11.

From Fig. 11, it can be observed that glass fiber on the surface of PA6-0 materials occurred, whereas little char residue was formed. The obtained charred layer was discontinued and had accidental agglomerations. Moreover, its thickness was also not uniform, which was in agreement with previous literature [33]. As a result, the quality of the total charred layer of GFPA6 composites was poor, which cannot effectively prevent transfer of heat, the penetration of oxygen and combustible gases. In contrary, for FR-GFPA6 system, the surface of the residue was smooth, compact, and tight, indicating a dense and continuous vitreous char layer structure. This vitreous char layer caused in a strong barrier effect against heat, degradation products of matrix polymer, and volatiles diffusion, leading to excellent flame retardancy of the FR-reinforced PA6 specimens. Besides, it can be observed that glass fibers, which can clearly reinforce steel bars in concrete, were regularly dispersed on the surface of layers and tightly combined with the char particles, and thus significantly improved the strength.

The qualitative elemental analysis of the selected area from the SEM images supports the generation of char in materials. Compared with pure matrix, the phosphorus element of the residue of PA6-4 increased to 18.1 mass%. This could produce many phosphorus-containing free radicals (as the radical scavengers), then combine with the segmental radicals generated from the heterolytic cleavage of PA6 to form compact char layer. Consequently, the presence of PAPP/AHP changed the decomposition mechanism of GFPA6 and induced the formation of cross-linking residue containing phosphorus, which can constrain the transfer of heat and oxygen and thus enhance the flame retardancy of FR-GFPA6 composites.

The flame-retarding mechanism of FR-GFPA6 composites

Figure 12 shows the experimental TG curves of PA6-1 (with 20 mass% PAPP), PA6-8 (with 20 mass% AHP) and PA6-4 in N_2 atmospheres, as well as the calculated TG curves of PA6-4 through overlapping the corresponding TG curves of 80 mass% PA6-1 and 20 mass% PA6-8 in N_2 atmospheres.

The comparison of the experimental and calculated TG curves of PA6-4 can provide the information about the accelerating degradation effects between PAPP and AHP. The thermal decomposition of PA6-1 was characterized by a single decomposition step from 330 to 500 °C, with the T_{max} at 377 °C and leaved 41.5 mass% residue formed at 700 °C. Meanwhile, the PA6-8 composite leaved 49.6 mass% char residue at 700 °C. It can be seen that the calculated curve of PA6-3 was far below experimental curve, showing remarkably accelerating carbon reaction in condensed phase. The experimental residue at 700 °C was increased to 46.2 mass%, which was 3.1 mass% higher than the calculated residue. The differences between experimental and calculated TG curves proved the strong interactions between the two components during degradation process. This change was mainly caused by the pyrophosphate and hypophosphorous acid formed from PAPP and AHP, contributing to the cross-linking reaction with caprolactam (or its oligomers) produced from the degradation of PA6, which finally resulted in the formation of a protective char layer. The interactions between PAPP and AHP leaded to obvious changes in the decomposition temperature and to increases in residue yield, convincingly confirming the better thermal oxidative stability of FR-GFPA6 system. Obviously, the partial replacement of PAPP by AHP effectively enhanced the thermal oxidative stability of FR-GFPA6 composites.

Figure 13 summarized the intensity of hydrocarbons for PA6-0, PA6-1, PA6-8, and PA6-4 composites. The introduction of PAPP clearly decreased the peak intensity comparing with PA6-0. It also can be seen that the curve of PA6-8 was below that of PA6-1, showing better flame-retarding efficiency. Comparably, the experimental curve

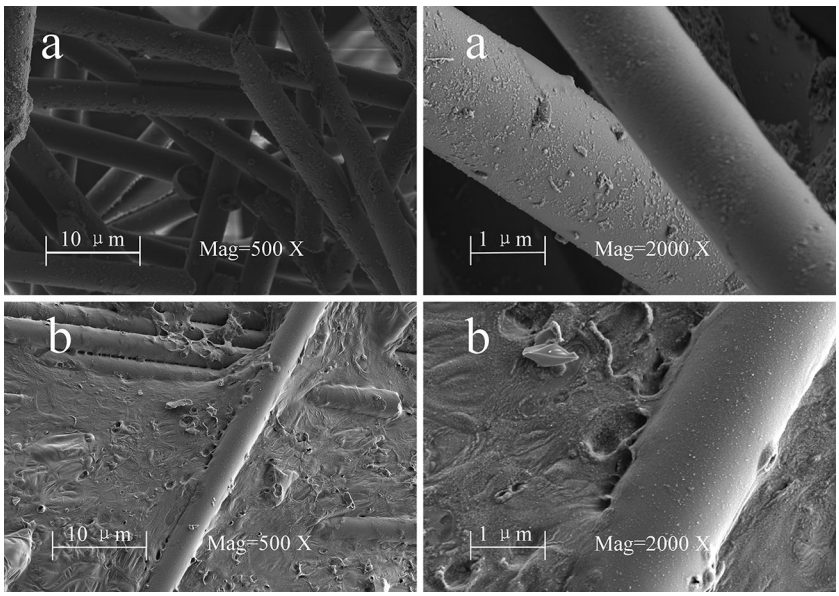

Fig. 11 SEM photographs of the residual charred layer of **a** PA6-0 and **b** PA6-4

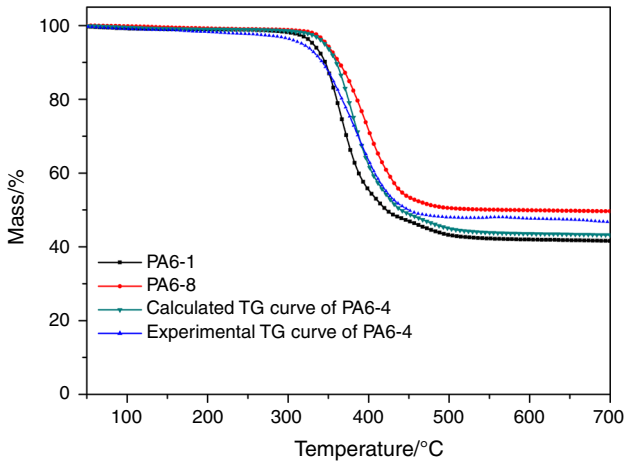

Fig. 12 Experimental and calculated TG curves of PA6-4

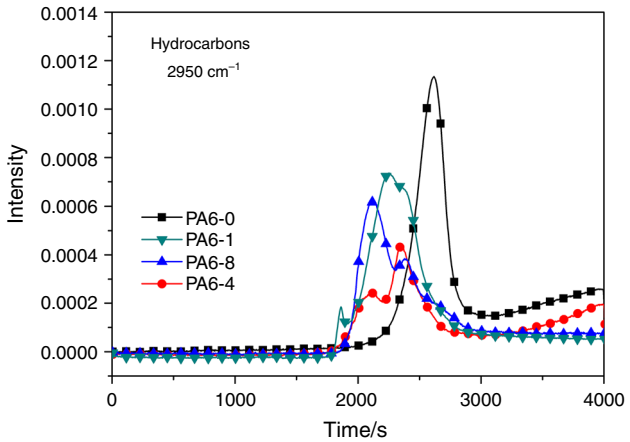

Fig. 13 Intensity of hydrocarbons of PA6-0, PA6-1, PA6-8 and PA6-4 composites

of PA6-4 was far below all the corresponding curves following the partial replacement of PAPP by AHP. This decrease may be ascribed to the interaction of PAPP and AHP, which can remarkably accelerate the cross-linking action with degradation products formed from PA6 matrix, quickly form a protective char layer and significantly reduce the release of combustible gas such as hydrocarbons. Obviously, the combination of PAPP and AHP effectively decreased the intensity of hydrocarbons in gaseous phase, which can be the flame-retarding mechanism in this system.

Consequently, the introduction of PAPP/AHP changed the decomposition pathway of GFPA6 and the evolved gas ingredients in the gaseous phase, contributing to the high flame-retarding efficiency.

Conclusions

PAPP was synthesized successfully. It was combined with AHP to flame retarded GFPA6 by the melt blending method. Comprehensive flame retardancy of FR-GFPA6 composites showed significant improvements. The experimental data of fire performance indicated that high LOI and V-0 classification can be achieved when the mass ratio of PAPP:MPP was 4:1. The char residue yield significantly was enhanced, the thermal stability of composites within high-temperature region increased, and the intensities of a variety of pyrolysis gas products correspondingly decreased following the introduction of PAPP/AHP on TG and TG-FTIR characterization. Continuous decrease in PHRR, THR, and shifted forward of ignition temperature through MCC test illustrated an interested decrease in

potential fire risk. The storage modulus of samples increased, whereas the T_g continued reduced owing to the existence of flame retardant. Furthermore, the incorporation of FR resulted in compact char layers without holes from SEM observation, which was ascribed to the cross-linking carbon reaction. The interaction of PAPP/AHP and GFPA6 during decomposition process induced the formation of cross-linking residue which contained phosphorus elements and had excellent barrier effect. Meanwhile, the carbon reaction between PAPP/AHP and GFPA6 decreased the release of combustible gases (PH_3 and hydrocarbons) was another flame-retarding mechanism in the gaseous phase.

Acknowledgements The work was financially supported by the Program for Science and Technology Talent of Shang Hai (15YF1405500) and the special development fund project of Shanghai Zhangjiang national innovation demonstration zone (201501-PT-C104-012).

References

1. Chen YH, Wang Q. Preparation, properties and characterizations of halogen-free nitrogen-phosphorous flame-retarded glass fiber reinforced polyamide 6 composite. Polym Degrad Stab. 2006;91(9):2003–13.
2. Harintharavimal B, Azman H. On the use of magnesium hydroxide towards halogen-free flame-retarded polyamide-6/polypropylene blends. Polym Degrad Stab. 2012;97(8):1447–57.
3. Monti M, Tsampas SA, Fernberg SP. Fire reaction of nanoclay-doped PA6 composites reinforced with continuous glass fibers and produced by commingling technique. Poly Degrad Stab. 2015;121:1–10.
4. Malchev PG, Vos GD, Picken SJ. Mechanical and fracture properties of ternary PE/GFPA6 composites. Compos Sci Technol. 2010;70(5):734–42.
5. Bernasconi A, Davoli P, Rossin D. Effect of reprocessing on the fatigue strength of a fibre glass reinforced polyamide. Compos Part Anal Appl Sci Manuf. 2007;38(3):710–8.
6. Tai QL, Richard KK. Iron-montmorillonite and zinc borate as synergistic agents in flame-retardant glass fiber reinforced polyamide 6 composites in combination with melamine polyphosphate. Compos Part Anal Appl Sci Manuf. 2012;43(3):415–22.
7. Aleksandra B, Timea S, Lea B. Bridged DOPO derivatives as flame retardants for PA6. Polym Degrad Stab. 2014;107:158–65.
8. Gijsman P, Steenbakkers R. Differences in the flame retardant mechanism of melamine cyanurate in polyamide 6 and polyamide 66. Polym Degrad Stab. 2002;78(2):219–24.
9. Hu Z, Chen L. Flame retardant of glass-fibre-reinforced polyamide 6 by a metal salt of alkylphosphinic acid. Polym Degrad Stab. 2011;96(9):1538–45.
10. Klatt M, Leutner B. Flame-retardant polyester molding compositions containing flame retardant nitrogen compounds and diphosphinates. U.S. Patent. 2003;503(6):969.
11. Zhao B, Li C. Aluminum hypophosphite versus Alkyl-substituted phosphinate in polyamide 6: flame retardancy, thermal degradation and pyrolysis behavior. Ind Eng Chem Res. 2006;45:8610–6.
12. Yang W, Song L. Enhancement of fire retardancy performance of glass-fibre reinforced poly (ethylene terephthalate) composites with the incorporation of aluminum hypophosphite and melamine cyanurate. Compos Part B Eng. 2011;42(5):1057–65.
13. Wu NJ, Li XT. Flame retardancy and synergistic flame retardant mechanisms of acrylonitrile–butadiene–styrene composites based on aluminum hypophosphite. Polym Degrad Stab. 2014;105:265–76.
14. Ge H, Tang G. Aluminum hypophosphite microencapsulated to improve its safety and application to flame retardant polyamide 6. J Hazar Mat. 2015;294:186–94.
15. Ulrike B, Bernhard S. Flame retardancy mechanisms of aluminium phosphinate in combination with melamine polyphosphate and zinc borate in glass-fibre reinforced polyamide 66. Polym Degrad Stab. 2007;92(8):1528–45.
16. Jenewein E, Kleiner HJ. Synergistic flame protection agent combination for thermoplastic polymers. U.S. Patent. 2002;365(6):071.
17. Chen T, Hao DM (2012) The preparation of piperazine pyrophosphate. China Patent. CN102304100A. vol 1.
18. Zhan ZS, Xu MJ. Synergistic effects of sepiolite on the flame retardant properties and thermal degradation behaviors of polyamide 66/aluminum diethylphosphinate composites. Polym Degrad Stab. 2015;117:66–74.
19. Nie SB, Peng C, Yuan SJ, Zhang MX. Thermal and flame retardant properties of novel intumescent flame retardant polypropylene composites. J Therm Anal Calorim. 2013;113:865–71.
20. Bakirtzis D, Ramani A. Simplified structure of the condensed phase of fire retarded PA6 nanocomposites in TG as related flammability. Fire Saf J. 2014;69:69–75.
21. Chen J, Liu SM. Synthesis, application and flame retardancy mechanism of a novel flame retardant containing silicon and caged bicyclic phosphate for polyamide 6. Polym Degrad Stab. 2011;96(8):1508–15.
22. Takashi K, Richard H. Flame retardant mechanism of polyamide 6–clay nanocomposites. Polymer. 2004;45(3):881–91.
23. Lyon RE, Walters RN. Screening flame retardants for plastics using microscale combustion calorimetry. Polym Eng Sci. 2007;47(10):1501–10.
24. Zhang J, Silcock GWH. Study of the combustion and fire retardancy of polyacrylonitrile and its copolymers by using cone calorimetry. J Fire Sci. 1995;13:141–61.
25. Pramoda KP, Liu TX. Thermal degradation behavior of polyamide 6/clay nanocomposites. Polym Degrad Stab. 2003;81:47–56.
26. Zou H, Yi C, Wang L, Liu H, Xu W. Thermal degradation of poly(lactic acid) measured by thermogravimetry coupled to Fourier transform infrared spectroscopy. J Therm Anal Calorim. 2009;97:929–35.
27. Perrer B, Pawlowski KH, Schartel B. Fire retardancy mechanisms of arylphosphates in polycarbonate (PC) and PC/acrylonitrile–butadiene–styrene. J Therm Anal Calorim. 2009;97:949–58.
28. Hu S, Song L. Thermal properties and combustion behaviors of flame retarded epoxy acrylate with a chitosan based flame retardant containing phosphorus and acrylate Structure. J Anal Appl Pyrolysis. 2012;97:109–15.
29. Wang BB, Zhou KQ. Enhancement on physical properties of flame retarded ethylene-vinyl acetate copolymer/ferric pyrophosphate composites through electron beam irradiation. Compos Part B Eng. 2012;43:641–6.
30. Mitra SM, Atul A. Investigation of accelerated aging behaviour of high performance industrial coatings by dynamic mechanical analysis. Prog Organic Coat. 2014;77(11):1816–25.
31. Masoud RA, Hossein AK. Application of mean-field theory in PP/EVA blends by focusing on dynamic mechanical properties in correlation with miscibility analysis. Compos Part B Eng. 2015;79:74–82.
32. Mofokeng JP, Luyt AS. Dynamic mechanical properties of PLA/PHBV, PLA/PCL, PHBV/PCL blends and their nanocomposites with TiO_2 as nanofiller. Thermochim Acta. 2015;613:41–53.
33. Zuo XL, Shao HJ. Effects of thermal-oxidative aging on the flammability and thermal-oxidative degradation kinetics of tris (tribromophenyl) cyanurate flame retardant PA6/LGF composites. Polym Degrad Stab. 2013;98(12):2774–83.